Article

Gold in the Oxidized Ores of the Olympiada Deposit (Eastern Siberia, Russia)

Sergey A. Silyanov [1,*], **Anatoly M. Sazonov** [1], **Yelena A. Zvyagina** [1], **Andrey A. Savichev** [2,3] **and Boris M. Lobastov** [1]

[1]   Institute of Mining, Geology and Geotechnology, Siberian Federal University, 79 pr. Svobodny, 660041 Krasnoyarsk, Russia; sazonov_am@mail.ru (A.M.S.); elena_zv@mail.ru (Y.A.Z.); lbm02@ya.ru (B.M.L.)
[2]   Department of Mineralogy, Crystallography and Petrography, Saint-Petersburg Mining University, 2 21st Line, 199106 St. Petersburg, Russia; a_savichev@mail.ru
[3]   LLC Norilskgeologia, 11 Grazhdanskiy Avenue, 195220 St. Petersburg, Russia
*   Correspondence: silyanov-s@mail.ru; Tel.: +7-963-188-9156

Abstract: Native gold and its satellite minerals were studied throughout the 300 m section of oxidized ores of the Olympiada deposit (Eastern Siberia, Russia). Three zones are identified in the studied section: Upper Zone ~60 g/t Au; Middle Zone ~3 g/t Au; Lower Zone ~20 g/t Au. Supergene and hypogene native gold have been found in these zones. Supergene gold crystals (~1 μm), their aggregates and their globules (100 nm to 1 μm) predominate in the Upper and less in Middle Zone. Relic hypogene gold particles (flattened, fracture and irregular morphology) are sporadically distributed throughout the section. Spongiform gold occurs in the Lower Zone at the boundary with the bedrock, as well as in the bedrock. This gold formed in the process of oxidation of aurostibite, leaching of impurities and its further dissolution. Hypogene gold is commonly isolated but for supergene gold typically associated with ferric (hydr)oxides. New formation of gold occurred due to oxidation of sulfide ores and release of "invisible" gold, as well as dissolution, mobilization and re-deposition of metallic hypogene gold. A model for the formation of oxidized ores with the participation of meteoric and low-temperature hydrothermal waters has been proposed.

Keywords: oxide ore; weathering; supergene gold; Olympiada gold deposit; Yenisei Ridge; mineral exploration

1. Introduction

Oxidized ores of gold deposits are important formations for the mining and metallurgical industry, as the weathering process leads to their partial enrichment and increased content of the noble metal. Moreover, oxidized ores do not require complex processing technologies and are profitable even at low grades. Commercially valuable oxidation zones of gold ores are known in Russia, Kazakhstan, Australia, Brazil and other countries [1–5].

In addition to the economic value, the oxidation zones of gold ore deposits are of fundamental interest due to the exogenous geochemistry and metallogeny of gold. Today there is a lot of evidence of gold mobility in supergene conditions in the form of various complexes [1,2,5–14]. Significant attention is also paid to the participation of bacteria in the remobilization and redeposition of gold [15–22]. The mobility of gold has been established in different climatic zones (subtropical, tropical, arid, humid, moderate, subarctic), including the permafrost zone [23–25].

Despite the progress made in understanding the mechanisms of gold behavior in exogenous conditions, some aspects remain controversial, both for specific deposits and in a broader sense. Most of them are about the way gold is transported and its mobility in the supergenesis zone, changes in the morphology and size, and bacterial participation in the remobilization and redeposition of gold. In this connection, there is a need to further study the process of oxidation of gold-sulfide ores. Therefore, the purpose of this research

was to study native gold in oxidized ores of the Olympiada deposit (Russia), as well as mechanisms of formation of supergene gold and its secondary enrichment.

The Olympiada gold deposit is a unique object in terms of the scale of mineralization with accumulated resources of about 80 Moz (about 2500 metric tons) of gold. Since 1985, just under 20 Moz metal has been mined at the deposit. According to PJSC Polyus, the proven and probable reserves as of 2020 comprise 24 Moz, and the estimated and identified resources comprise 39.4 Moz of gold.

The Olympiada deposit is unique also in terms of the scale of the gold-bearing oxidation zone developed within it. In terms of the depth of its distribution (over 400 m from the recent surface), the deposit has no analogs among gold projects of the world. Oxidized ores of the deposit were mined from 1985 to 2007. During this period, about 17 Mt of ore with an average grade of ~11 g/t was mined, which in terms of pure metal was about 193 tons [26].

In our recent work, we provided a general review of geology and primary (hypogene) sulfides ore of the Olympiada gold deposit [26]. However, oxidized ores have not been described since 2003. Therefore, our present work is devoted to the description of gold of the oxidized ores of the deposit.

Studies of oxidized ores of the Olympiada deposit allowed new data to be obtained on the morphology, chemical composition and gold differentiation in the stratum (at a depth of ~300 m) of oxidized ores, as well as proposing a model of supergene redistribution of noble metal and other elements in the oxidation zone.

2. Geological Setting of Olympiada Deposit and Characteristics of Sulfide Ores

2.1. Geological Setting

The Olympiada deposit is located in the center of the Yenisei Ridge (Eastern Siberia, Russia), which is a Neo-Proterozoic (860–800 Ma) collision orogen. The latter has passed to the riftogenic stage of development at the boundary of ~750–680 Ma [27], which coincides with the age of gold-sulfide and gold-antimony mineralization [28].

The deposit is confined to the silicate and carbonate band of the Lower Riphean Kordinskaya suite clastic stratum. Granitoids located 2.5 km away from and above the deposit surround it. The structure of the ore field is an ensemble of conjugated W-shaped folds (Figure 1).

2.2. Primary (Hypogene) Sulfide Ore

The main reserves of the deposit are concentrated in bedrock hypogene ores (average gold grade 4.0–4.6 g/t). When additional exploration of deep horizons of the deposit was carried out, ore intersections with commercial grades at depths of over 1500 m were recorded.

Sulfides (2 to 7%), which gold is associated with, are developed in quartz (30–45%)–mica (20–35%)–carbonate (35–40%) rocks. More than 50 hypogene ore minerals have been found at the deposit, among which arsenopyrite, pyrrhotite, pyrite, stibnite and berthierite prevail. They are present in the form of dissemination of submillimeter and submicron grains in metasomatites and more rarely in pocket-like inclusions in quartz segregations. The earliest ore minerals (Au-As association) are needle-shaped arsenopyrite, pyrite, pyrrhotite and chalcopyrite. The Au-Sb $\pm$ (Pb-Ag-Hg-W) association, represented by stibnite, berthierite, mercurous gold, aurostibite, jamesonite, gudmundite, late arsenopyrite and rarely scheelite, has been identified with time lag. Mercury minerals, mainly coloradoite, are also noted here [35]. Gold-arsenic and gold-antimony ores are the main ore components.

On the surface, the Olympiada deposit consists of two spatially separated parts, Western and Eastern Olympiada, which are joined at the depth of the Intermediate part. The deposit is located within the complex Medvezhinskaya anticline complicated by a junction of broadly E–W, NE and NW faults. The core of the fold is composed of quartz-two-mica schists, and the limbs are formed by quartz-mica-carbonate (with layers and

lenticular layers of marbled limestone) and quartz-mica-carbonate schists (Figure 1). Ore bodies of the deposit are confined to the limbs and joint part of this block-folding structure. The result of the different positions of the Western, Intermediate and Eastern sections in it is their abrupt difference in the scale of mineralization, 90% of which (including oxidized ores) falls on the Eastern Olympiada. The geology of the Olympiada deposit is described most fully in the works [26,29–34].
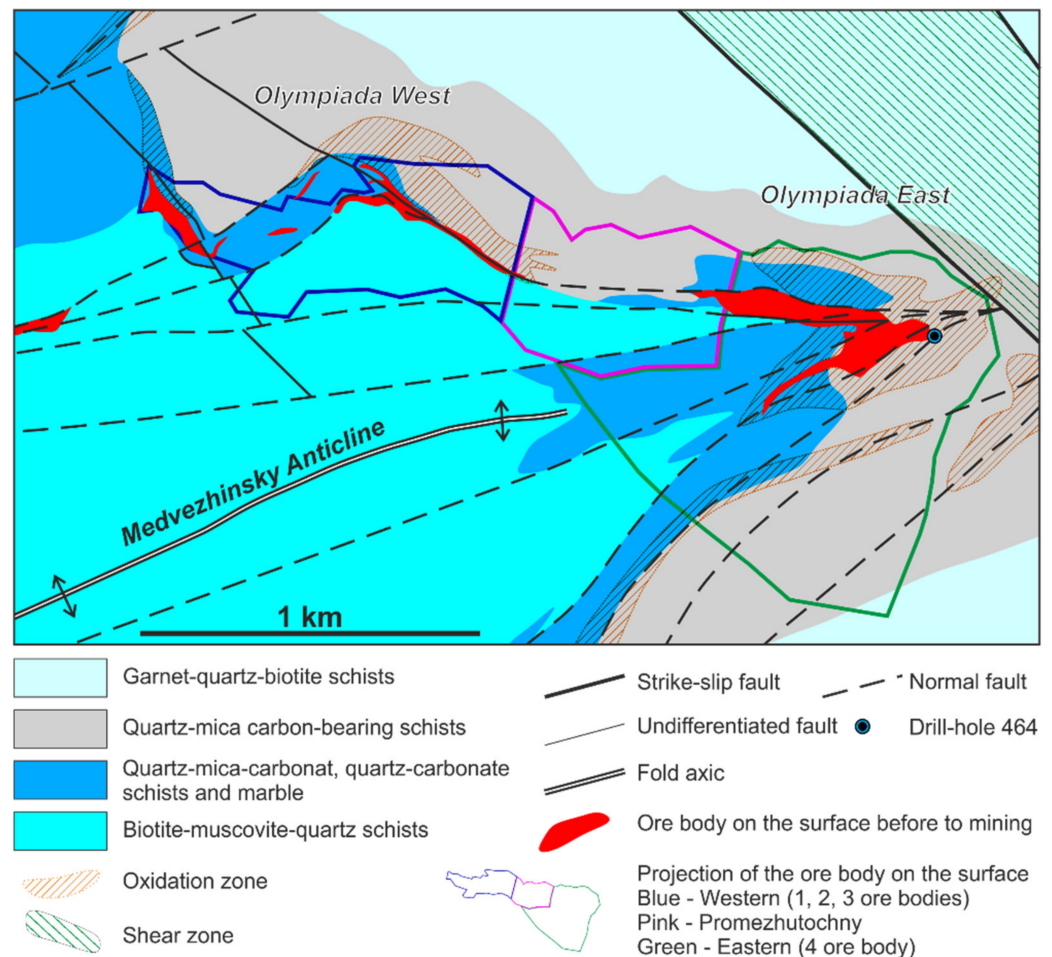
Figure 1. Geological map of the Olympiada gold deposit [26].

Gold in bedrock ores. The gold grade in the ores varies from 0.n to tens of g/t. Gold is mainly fine, pulverized, with a predominant size of about 10 μm (coarse, pocket-like inclusions accompanied by hurricane concentrations reaching kg/t are noted). The form of inclusions is irregular, lamellar, vein-shaped, fracture, droplet-shaped and spongiform. In the ore milled down to −74 μm, about 15% of gold is in a free form, and up to 45% is in a cyanidable form in aggregates with ore minerals [34,36]. The most common gold inclusions in quartz and sulfides are arsenopyrite, pyrite, pyrrhotite and berthierite (Figure 2). Native gold of the early Au-As association is high in fineness (880–1000‰, 970‰ on average); mercury and silver, and less often copper, are present as impurities. In antimony ores, the gold fineness decreases to 647–757‰ due to the increased concentrations of Hg, Cu, Ag, as well as the occurrence of aurostibite, and increases to 1000‰, when spongiform gold replaces aurostibite.
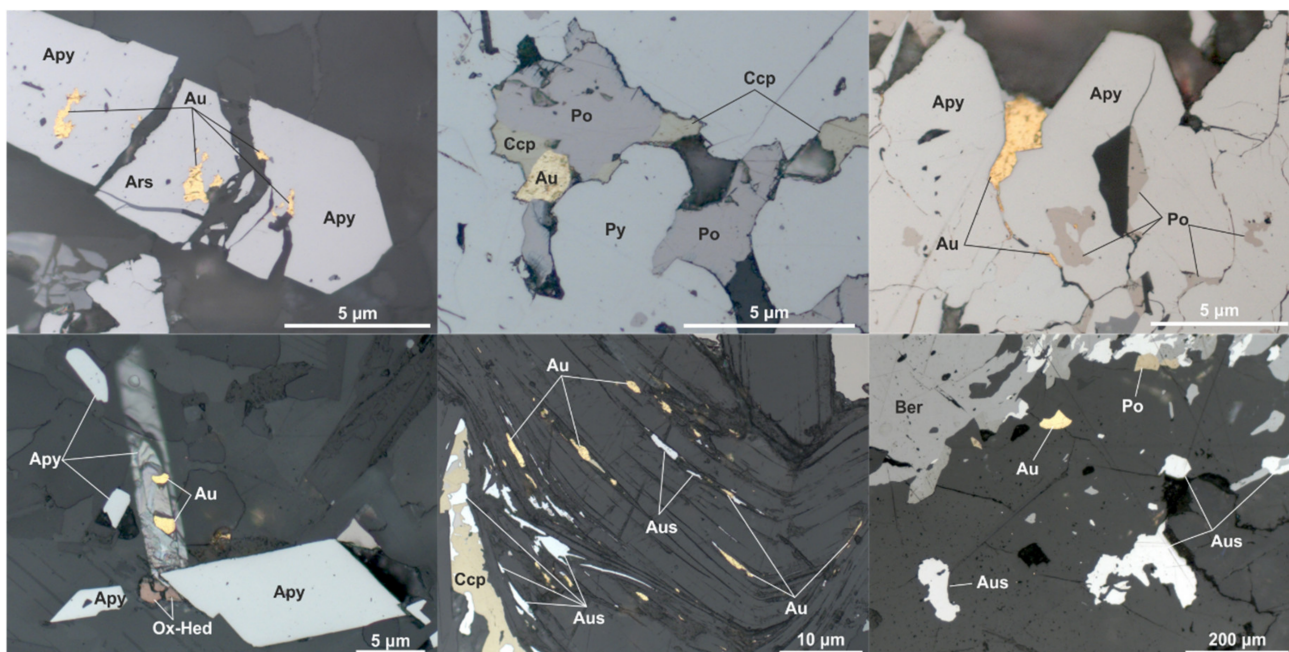
Figure 2. Native gold in primary (hypogene) sulfide ore (optical photo). Apy—arsenopyrite, Au—gold, Aus—aurostibite, Po—pyrrhotite, Py—pyrite, Ccp—chalcopyrite, Ox-Hed—oxidized hedleyite, Ber—berthierite.

In addition to micro- and macroscopic gold, the ores contain "invisible" (refractory) gold, which is not extractable by cyanidation. The share of such gold can reach 40–60%, and its extraction is carried out by JSC Polyus Krasnoyarsk using its own bio-oxidation technology BIONORD® [36]. "Invisible" gold is confined to sulfide minerals of the deposit, first of all, to needle-like arsenopyrite of the early association, in which its concentrations range from 0.0n to 2298 ppm [37,38]. According to modern ideas, "invisible" gold in arsenopyrite is present in the form of nanosized Au^0 inclusions and in a structurally bound form [38–40]. Earlier Mössbauer studies on ^{197}Au atoms for gold-bearing arsenopyrite of the Olympiada deposit showed that the content of structurally bound and nanosized metallic gold varies between 3 and 45% and 55 and 97%, respectively [37].

2.3. Oxide (Supergene) Ore

The oxidation zone of primary sulfide ores within the Eastern Olympiada covered almost the entire area of the ore body (about 45,000 m^2) and reached a depth of more than 400 m from the current surface. In vertical sections, the gold-bearing oxidation zone represented a large column-shaped body (Figure 3), which gradually decreased in size with depth and thinned out in full at horizon +280 m. The gold grade in oxidized ores reached 447.2 g/t. The geochemical spectrum of the Olympiada oxidized ores was characterized by a close correlation of Au with W, Sb, Hg, less often with Ag and Pb, but not with As. Thus, at a horizon +600 m, the average grades (ppm) and concentration coefficients with respect to the primary ores were equal: for Au to 9.9/3.1, for Ag to 0.3/2.8, for Sb to 2228.0/2.5, for Hg to 43.6/4.4, for Pb to 261.0/11.3, for W to 677.0/11.6 and for As to 681.0/0.9.

In the north, in the broadly W–E segment of the ore body of the Eastern Olympiada, the oxidation zone was characterized by lower (up to 130 m) thickness and actually repeated the geochemistry of the primary Au-As-(Sb) ores in terms of the grade and distribution of these and other elements, while not demonstrating noticeable supergene enrichment. In the zone of the Main NE Fault, oxidized ores had the much higher thickness and productivity for gold; subvertical "ore shoots" were distinguished in them [30], containing more than 50 g/t of Au and abruptly enriched the W, Pb, Ag and Sb [31]. Here, oxidized ores were developed mainly after antimony primary ores (Figure 3a). The thickest and highest-grade chimney-shaped body, going down to a depth of 400 m, was characterized by an

abnormally high grade of mercury (up to 0.2 wt.%) and antimony (up to 1.0 wt.%), but a lower grade of As, as well as Ti, Fe, Cr and other siderophiles. Marshallites prevailed in it. These are poorly cemented rocks of gray tints, consisting mainly of quartz (60–85%) and "hydromica", colored by scattered organic matter (up to 1.6%) (Figure 4). Quartz grains, as well as accessory minerals—zircon, tourmaline, and even a number of fine gold grains, often had a spherical shape in marshallites [41].
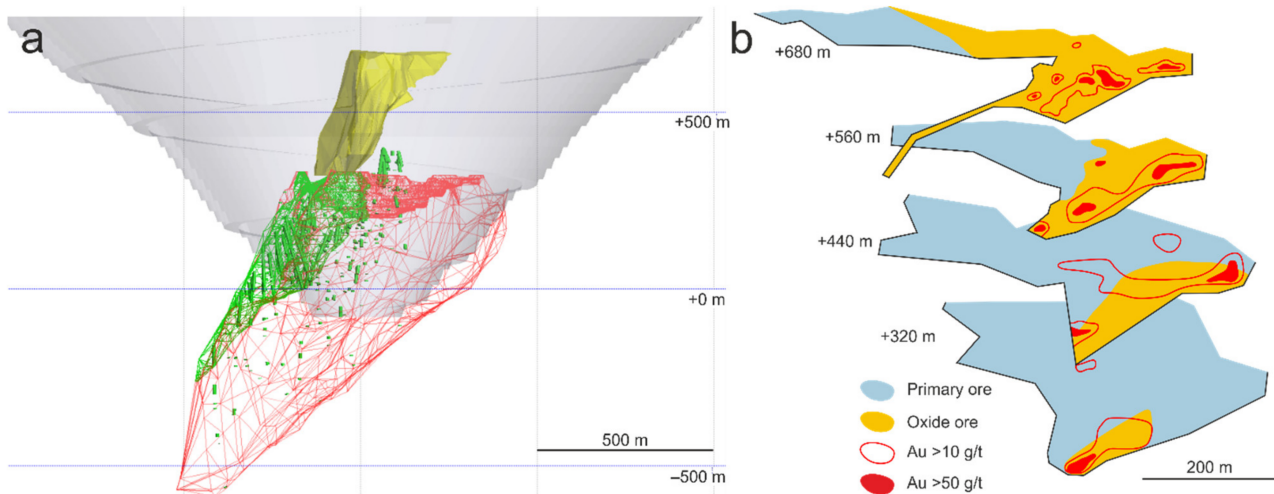
Figure 3. Eastern Olympiada. (**a**)—3D model: yellow—oxidized ores, green—gold-antimony ores, red (frame)—gold-arsenic ores, gray—pit outline; (**b**)—horizon plans of the ore body [30].
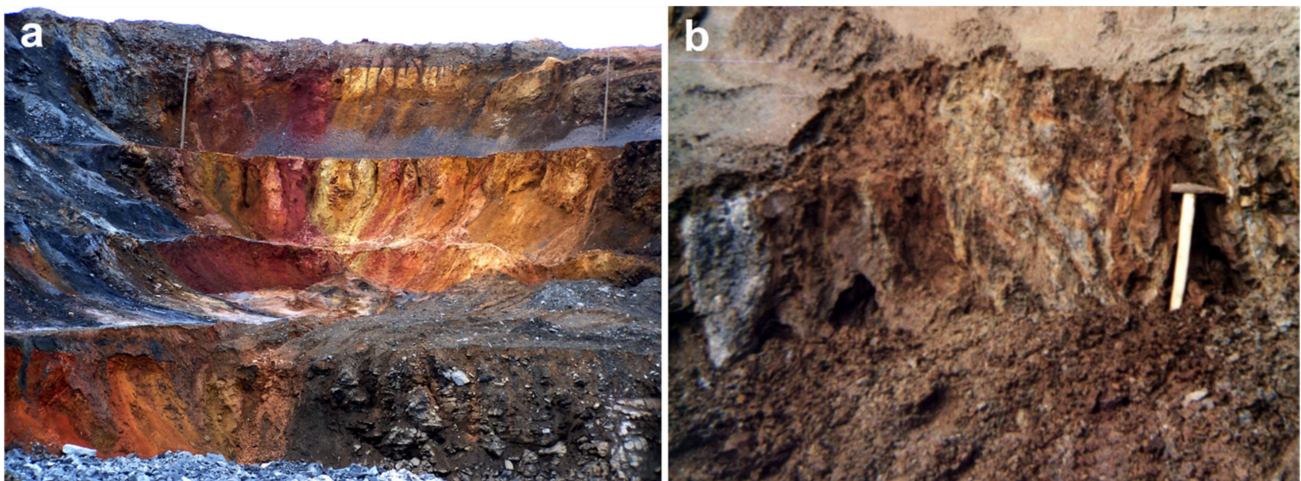
Figure 4. Oxidized ores of the deposit. (**a**)—General view of oxidized ores in the Eastern Olympiada pit (photo by S.A. Kamenev, 2004); (**b**)—outcrop of oxidized ("hydromica") ores with a marshallite body at horizon +580 m (photo by A.A. Savichev, 1999).

Typical "hydromica" oxidized ores of the Olympiada deposit were colored in different tints of brown, red, dark gray, orange, and contrasting isolated rocks [42,43] (Figure 4). In terms of the particle size distribution, the clay fraction prevailed in them (64%), and the smaller part was represented by the debris (10%), sandy (10%) and aleurtic fraction (16%). The mineral composition of oxidized ores had been studied before [41–45]. The main minerals were "hydromica" (40–70%), ferric hydroxides (1–36%), quartz (5–35%), kaolinite (up to 14%) and chlorite (up to 10%). There were relic epidote, calcite, biotite, actinolite, chloritoid, clinozoisite, garnet, plagioclase, staurolite, sillimanite, zircon, rutile, anatase, brookite and titanite.

Oxidized ores contained up to 10% of ore minerals, among which more than 30 species (excluding relic sulfides) were identified. Ferric and manganese oxides (hematite, lepidocrocite) and hydroxides prevailed, while antimony (senarmontite, cervantite, valentinite, "stibiconite") and tungsten (tungstite, hydrotungstite) oxides and hydroxides were rarer. Among manganese minerals, lithiophorite, todorokite and psilomelane with elevated concentrations of Ba (up to 3.0 wt.%), Co, Cu, Ni, Zn ($0.n$ wt.%) and REE (0.03–0.04% in lithiophorite) are described. The impurities of As (up to n%), P, W and Hg ($0.n$ wt.%) were present in the composition of sinter goethite. Scorodite, litharge, cerussite, anglesite, gypsum and baryte were also defined [46,47].

The typical feature of oxides and hydroxides of oxidized ores was wide isomorphism in the cation part between Sb, W, Pb and Hg. Thus, the W grade reached 5–10 wt.% in tripuhyite (up to 23.6 wt.%), and in "stibiconite" it was up to 16.8 wt.%, including 1.2 wt.% of Au. Abnormally high W grades (7.6–8.0 wt.%) were typical for cesàrolite [46]. In spite of the diversity of tungsten concentrator minerals, the main carrier in the oxidation zone was a newly formed scheelite, which differed significantly from scheelite from the primary ores in its REE distribution, and contained fluid inclusions with a homogenization temperature of 197 °C, which is important in genetic terms [47].

Gold from the Olympiada oxidation zone, according to a number of previous studies, is finely dispersed [43–45]. Most of it (63.7–91.8%) is concentrated in class −74 µm, and coarser gold (up to 0.5 mm) makes no more than 4–5% [45,48,49]. According to [45,48,49], a significant portion of gold (78.3–92.1%) is associated with ferric hydroxides, and 0.9–3.1% of Au is in a water-soluble form. In oxidized ores, there is relic primary and newly formed gold [45].

Secondary residual gold is formed in situ during the oxidation and decomposition of gold-containing minerals. It is closely associated with antimony and ferric hydroxides: its micro-particles are present in goethite pseudomorphs after arsenopyrite crystals. Spongiform and veinlet aggregates, lumpy gold grains and filamentous inclusions several µm in size are found in tripuhyite and bindheimite, which replace berthierite. As A.D. Ginkin [45] shows, the etching of such gold grains clearly demonstrates recrystallization structures. Secondary redeposition of gold is rare and associated with local infiltration accumulations of antimony oxides in the upper part of the oxidation zone. Redeposited gold is associated with sinter tripuhyite and "stibiconite", which fill fractures in weathered metasomatites. Gold is present as 0.3–4.0 µm globules scattered on the surface of cryptocrystalline tripuhyite balls. Gold from the oxidation zone is high in fineness (>980‰). The impurities include mercury (0.1–3.7 wt.%) and Ag, Cu, Mn, W and Sb in quantities up to 0.2 wt.% [45]. According to P.V. Bernatonis [43], the average composition of gold from the oxidation zone is (wt.%): Au 94.74, Ag 3.05, Hg 1.63, Fe 0.33, Sb 0.12, and Cu 0.02.

The genesis of the oxidized ores at the deposit is under discussion. According to one model, the oxidized ores belong to supergene products of the linear weathering crust of the Cretaceous–Paleogene age after mineralized carbonate and carbonaceous rocks [42,44]. Another one suggests the occurrence of low-temperature hydrothermal activity up to the Holocene age [41].

3. Samples and Methods

We studied 27 samples of oxidized ores of the Olympiada deposit, collected from Drillhole 464 located in the eastern part of the Eastern section of the deposit (Figure 1). The drillhole was drilled vertically and intersected the entire stratum of oxidized ores, stopping in the structural eluvium of the bedrock. The samples were collected from the depth range of 48–302 m and represent material of clay sizes with different shades of brown, red and gray colors (Figure 4).

Mineralogical studies were performed using SEM Tescan Vega III SBH with EDS Oxford X-Act in the R&D Nornickel SibFU Krasnoyarsk, Russia (analysts S.A.S and L.B.M.). The analytical conditions were the following: accelerating voltage of 20 kV, beam current of 1.2 nA and 60 s measuring time; pure elements (Au, Ag, Cu, Mn, W), as well as FeS_2,

FeAsS, SbS$_2$, SiO$_2$, Al$_2$O$_3$, K(AlSi$_3$O$_8$) and CeO$_2$, were used as standards; detection limit was 0.05%.

Trace elements (Ag, W, Sb, Ce, Pb, Cu) were determined with the ICP-MS method in the Agilent 7500cx device manufactured by Agilent Technologies. The sample weighted portion was preliminarily transferred by progressive digestion into nitric-acid and aqua regia solutions, which allowed it to be kept in the liquid phase and for analyzing the maximum possible set of elements to be analyzed. The quality of the obtained results was estimated on the basis of rock and ore standards BCR-2, BHWO, SSL-1. The analyses were performed in the common-use Analytical Center of Geochemistry of Natural Systems of the Tomsk State University, Tomsk, Russia.

The gold grade is given according to the data of the fire assay carried out in the laboratory of JSC Polyus Krasnoyarsk, Krasnoyarsk, Russia.

The bulk X-ray analysis was performed using CuKα radiation on polycrystalline X'Pert PRO diffractometer (PANalytical) with a PIXcel detector equipped with graphite monochromator in the Institute of Chemistry, Siberian Branch of the Russian Academy of Sciences, Krasnoyarsk. The dish with the sample was placed in a standard position. The survey was performed for reflection with the sample rotation at 360°/s. The survey range was from 5 to 101° on the 2θ scale, with a 0.026° spacing, Δt = 50 s.

4. Results

4.1. Structure of the Oxidized Ore Section

There are three zones in the studied section of oxidized ores of the deposit. The upper part of the section (Upper Zone) from 0 to ~135 m is characterized by saturated orange, red-orange color, which turns into gray-brown with depth (towards the zone boundary). The middle part of the section (Middle Zone) from a depth of ~135 to ~213 m has a gray-brown color with a yellowish tint in the roof, which changes to light gray-brown and dark raspberry-red towards the bottom. The bottom of the section (Lower Zone) to a depth of ~300 m has the most uniform brown-yellow color, which becomes slightly darker with depth. Below 300 m there are weathered rocks of gray-blue color in the oxidized ore section (Figure 5).

The mineral composition of the oxidized ores is variable in these zones. The Upper Zone is characterized by approximately equal ratios of quartz and "hydromica" in the absence of kaolinite. The Middle Zone contains more layered silicates (about 2/3 by weight), while the amount of kaolinite increases abruptly at the boundary with the Upper Zone and gradually decreases towards the Lower Zone, which is similar in terms of minerals to the Upper Zone. In terms of the structure, the studied oxidation zone differs from the classical one, where the top of the section should contain a hydrolysis zone maximally enriched with kaolinite and "hydromica" [50].

The Au grade in the studied samples varies from 0.2 to 61.1 g/t, and its distribution across the section is not uniform. The upper part of the section (Upper Zone) is the highest-grade, where the amount of Au increases abruptly to ~60 g/t. In the Lower Zone, high (~20 g/t) metal grades are also observed. The Middle Zone is characterized by a variable Au grade from 0.2 to 7.0 g/t. Meanwhile, the boundaries of the identified zones are traced by a sudden change in the metal grade (Figure 5).

The share of Ag does not exceed 1.5 g/t, and the minimum grades have been identified in the bottom of the section and the maximum grades at the top. Antimony and tungsten are characterized by similar distribution throughout the drillhole section. The metal grade in all zones is quite high (250–1750 g/t of Sb and 30–150 g/t of W). However, there is an abrupt decrease in their grade at the zone boundaries (Figure 5).
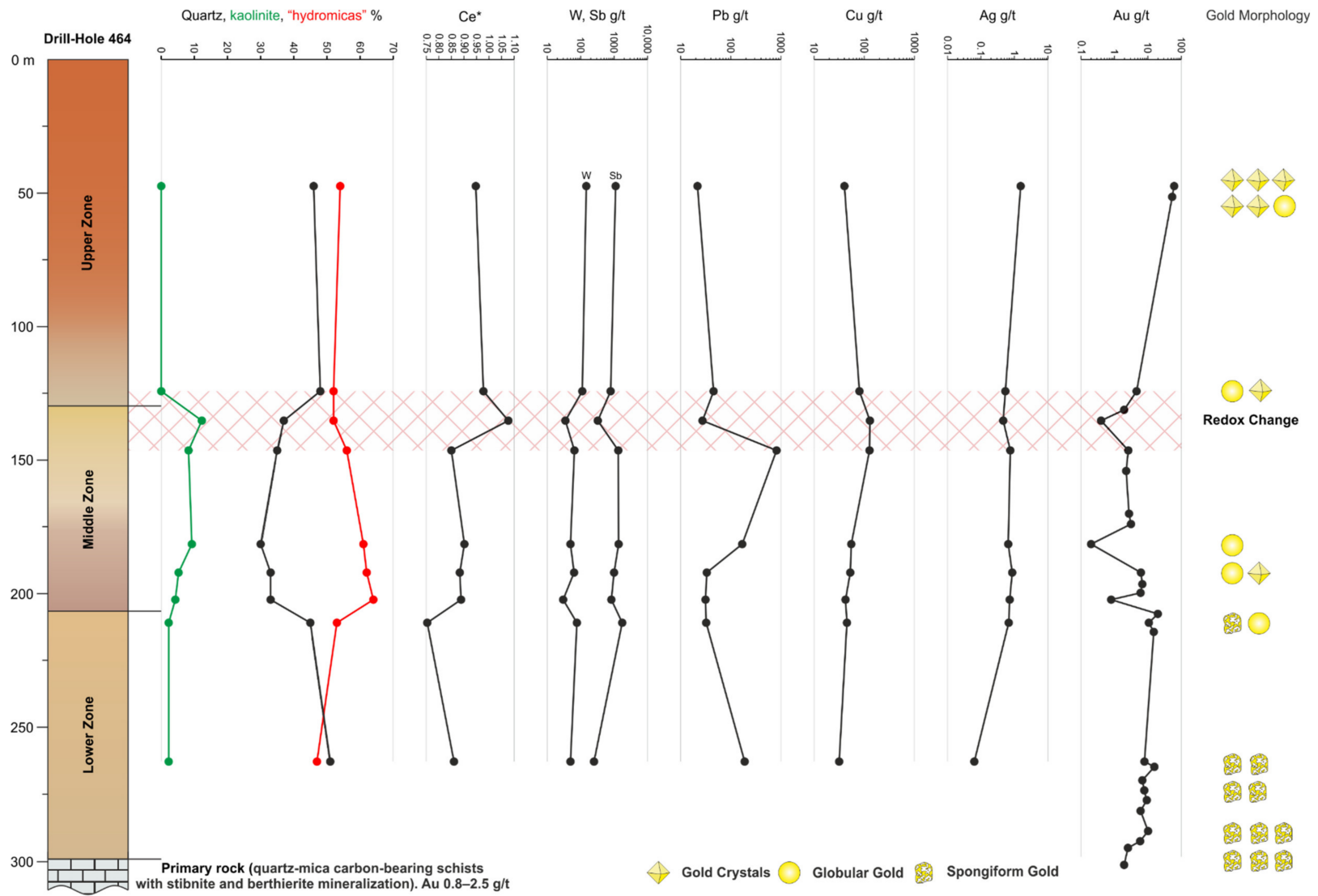
Figure 5. Structure of the oxidized ore section.

4.2. Mineralogy of the Studied Section of Oxidized Ores

The studied samples of oxidized ores consist of quartz, "hydromica", kaolinite and ferric (hydr)oxides. In addition to them, relic chloritoid, chlorite, monazite, rutile, scheelite and tourmaline are present in small quantities. Relics of sulfides oxidized from the surface (pyrite, pyrrhotite, arsenopyrite, stibnite) have been found in single quantities.

Supergene minerals include cervantite ("stibiconite" ?, valentinite ?), tungstibite, tungstite, hydrotungstite, tripuhyite, coronadite, bindheimite, plattnerite, oxyplumboroméite and oxy-calcioroméite (Figure 6a–c, Table 1). In several cases, obviously newly formed cerium oxide (cerianite-(Ce)) was found in association with ferric (hydr)oxides and manganese oxides at the Middle and Upper Zone boundary (intervals 125.0–126.5 and 132.0–134.0). The morphology of supergene mineral formations is mainly nodular, sinter and globular; irregularly shaped granular aggregates are observed less frequently (Figure 6d). The size of individual globules and microcrystals of these minerals is usually 1–2 μm or less. Often, the newly formed cerianite-(Ce) forms grains of quartz or other minerals. Samples with numerous findings of cerianite-(Ce) differ in the increasing value of the ceric anomaly up to ~1.08, with its general negative nature in the Middle and Lower Zones (~0.75–0.90).
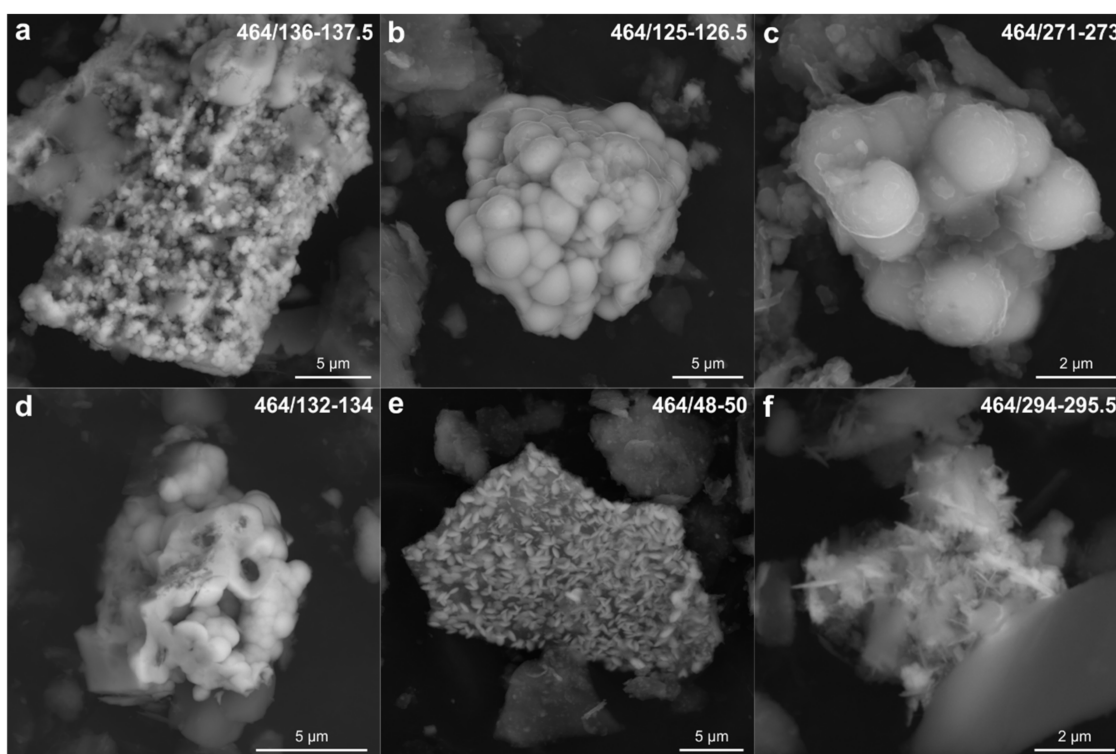
Figure 6. Supergene minerals of oxidized ores. (**a**)—globular tungstibite; (**b**)—nodular cervantite; (**c**)—nodular oxy-calcioroméite (?); (**d**)—nodular cerianite (Ce); (**e**)—flakyd lepidocrocite (?) after quartz; (**f**)—needle-like inclusions of montroydite (?).

The predominant supergene ore minerals are ferric (hydr)oxides (lepidocrocite, goethite, hematite, etc.), which almost always contain the As (0.4–3.2 wt.%), S (up to 2.1 wt.%), W (0.2–3.0 wt.%), Sb (0.5–4.9 wt.%) and P (0.2–1.3 wt.%) impurities. In this case, the W impurity and the elevated concentrations of Sb and As are noted mainly in the upper part of the section. The maximum S and P grades are typical for the Middle Zone. The morphology of ferric (hydr)oxide inclusions varies from sinter forms after relic minerals to flaky and scaly inclusions (Figure 6e), as well as split crystals. Most often, secondary ferric minerals grow on the nuclei of relic quartz and mica, but their individual grains and aggregates are also often found. Secondary arsenic minerals (scorodite and phases with similar composition) were founded in the films on the oxidized arsenopyrite grains.

Table 1. Normalized average chemical composition of supergene minerals of oxidized ores (wt.%).

Mineral Name	O	Mg	Al	Si	Ca	Mn	Fe	Co	Ni	Sb	W	Pb	Ce	Sum
Cervantite (n = 2) [1]	20.9	2.4		1.0			0.5			75.2				100
Oxycalcioroméite (n = 2)	25.9		1.0		11.6		4.6			56.9				100
Tripuhyite (n = 3)	25.1		2.2	3.8		0.4	23.0			45.5				100
Tungstite (n = 4)	21.9		2.1				4.3				71.7			100
Hydrotungstite (n = 2)	26.0		3.1				3.3				67.6			100
Tungstibite (n = 2)	20.2									44.1	35.7			100
Plattnerite (n = 2)	15.0						0.5					84.4		100
Bindheimite (n = 2)	17.3									32.3		50.5		100
Oxyplumboroméite (n = 2)	19.2				5.0		3.6			39.2		33.0		100
Coronadite (n = 3)	38.8					31.7	3.6				3.1	22.9		100
Cerianite-(Ce) (n = 4)	17.3						2.6						80.2	100

[1] (n = 2)–number of analyses.

In the lower part of the section of the oxidized ores stratum (Lower Zone), aggregates of crystals of needle-like and near-isometric, tetrahedral morphology (Figure 6f) were observed, in which Hg (52.0 wt.%) and O (23.0 wt.%), as well as S (11.3 wt.%), Cu (7.7 wt.%) and Fe (4.1 wt.%), prevailed. It is assumed that a needle-like mineral is a rhombic mercury oxide montroydite. Its formation is possible during oxidation of coloradoite and/or some minerals of the polymetallic sulfides stage associated with chalcopyrite (probably its relic in Figure 6f in the form of tetrahedral crystals with an even surface of faces) and carrying the isomorphic impurity of mercury—sphalerite, tetrahedrite, berthierite, jamesonite— in which the impurity of Hg up to ~1690 ppm is noted according to LA–ICP–MS. The formation of montroydite may be associated with oxidation of native mercury, the findings of which have been repeatedly observed at the Olympiada deposit [26].
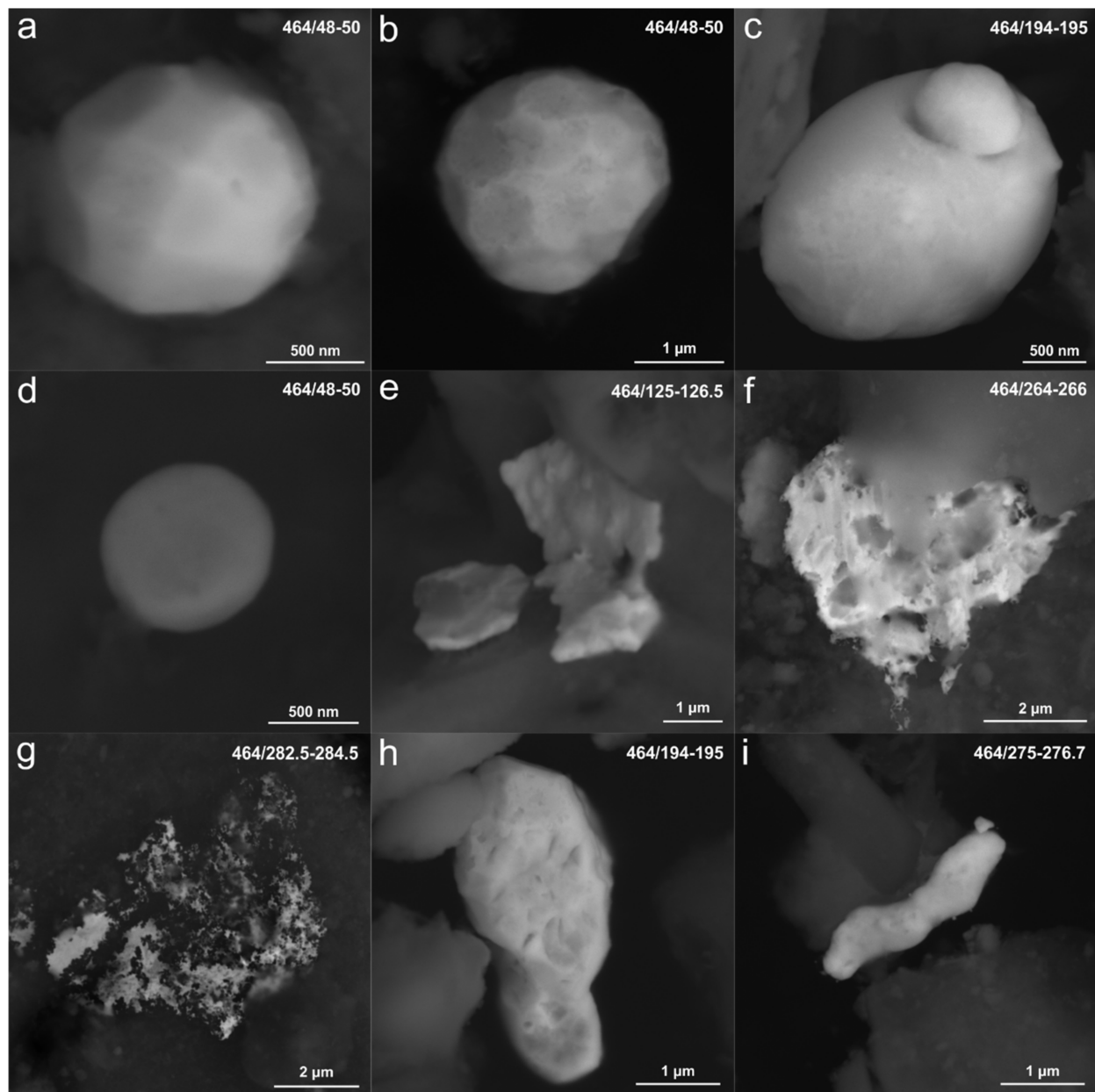
4.3. Native Gold in Oxidized Ores

More than 300 particles of supergene and relic native gold of different morphology ranging in size from ~30 nm to ~5–7 μm, rarely more, were found in the studied samples of oxidized ores of the deposit. The distribution and amount of free gold particles are consistent with its bulk gold grade in the samples.

Obviously newly formed isometric crystals of native gold were often observed (Figure 7a, Figure S1). Their size is uniform, 1.3 μm in diameter on average, with variations from 1.0 to 1.7 μm (sometimes up to 2.5 μm). The cutting of crystals has several simple shapes—usually a combination of a cube {100}, octahedron {111} and rhombodecahedron {110}; facets of a tetragon-trioctahedron {hhl} (?) often supplement them. In a single case (Figure 7b), all shpes possible for the *m3m* symmetry type are observed—tetrahexahedron, trigontrictahedron and hexoctahedron (Figure S1), in addition to the specified ones.

Globular particles may be attributed to the following morphological type of supergene gold (Figure 7c, Figure S2). The diameter of the most representative globules varies from 1.2 to 2.3 μm. The surface of these formations seems to be slightly rough or nanoporous. The same group includes rounded particles of subnanometer size (20 to 50–800 nm), due to which it is difficult to distinguish their true shape. Such nanoformations of native gold are very common. Single disc-shaped particles (Figure 7c, Figure S2) with a diameter of ~1 μm and a visible thickness of about 250 nm were discovered, which can be crystals flattened along one of L_4 and apparently supergene.

Considerably large sizes (~4–5 μm, thickness within 100–200 nm) are typical for rare particles of irregular morphology, which are probably relic gold (Figure 7e, Figure S3). Their peculiar contours suggest that they are fracture inclusions of hypogene gold of primary sulfide ores.

Figure 7. Morphology of native gold in oxidized ores. (**a**,**b**)—crystals; (**c**)—globular gold; (**d**)—disc-shaped gold; (**e**)—relic gold; (**f**,**g**)—spongiform gold; (**h**)—gold of irregular morphology; (**i**)—worm-shaped gold.

One of the most common morphological types is spongiform gold (Figure 7f,g, Figure S4). The size of such gold grains varies within the widest range from ~1 to ~6 μm and above. The contours of the grains are irregular, "torn" and porous. The sizes of branched mineral particles and cavities are within 20–100 nm. This is probably relic gold, which was subjected to the removal of impurities and partial dissolution. One of the mechanisms of its formation can be the replacement of aurostibite, which is common in the primary ore paragenesis, with extremely high-grade gold and stibnite, which was later oxidized to senarmontite, cervantite and valentinite. The latter, while being washed out, left spongiform cavities.

Irregularly shaped gold is found with traces of chipped mineral inclusions (?), with sizes in the range of 1–4 μm (Figure 7h, Figure S5). It may be assumed that this is also relic gold of primary ores, but it may also be crystals with less pronounced cut and induction surfaces. A single worm-shaped gold grain (Figure 7i) with dissolution traces (?) was also noted.

The distribution of the main (most common) morphological types of gold in the section is not homogeneous (Figure 5). Thus, most of the gold crystals are confined to the Upper Zone. In the middle part of the section, single crystals are observed, while there are none in the lower part of the section. In contrast to gold with crystallographic cut, spongiform gold is mostly found in the lower part of the section, closer to the bedrock. Gold with irregular morphology demonstrates the same tendency. Globular gold is found in single quantities in the Upper and Middle Zones and is most often found at the boundaries of geological and geochemical zones. Few relic gold grains are sporadically found throughout the section.

In the sample collected from weathered bedrock underlying the oxidized ores of the deposit, calcite aggregates with inclusions of antimony oxidized minerals and spongiform different fineness gold (Figure 8) were found. Here, spongiform gold with antimony impurity (up to ~38 wt.%) and presumably cervantite are noted in close aggregation. The formation of this association is possible during the decomposition of aurostibite and/or aurostibite and the coexisting antimony (stibnite) minerals. Such formations probably correspond to the initial stage of weathering of gold-antimony ores of the deposit.
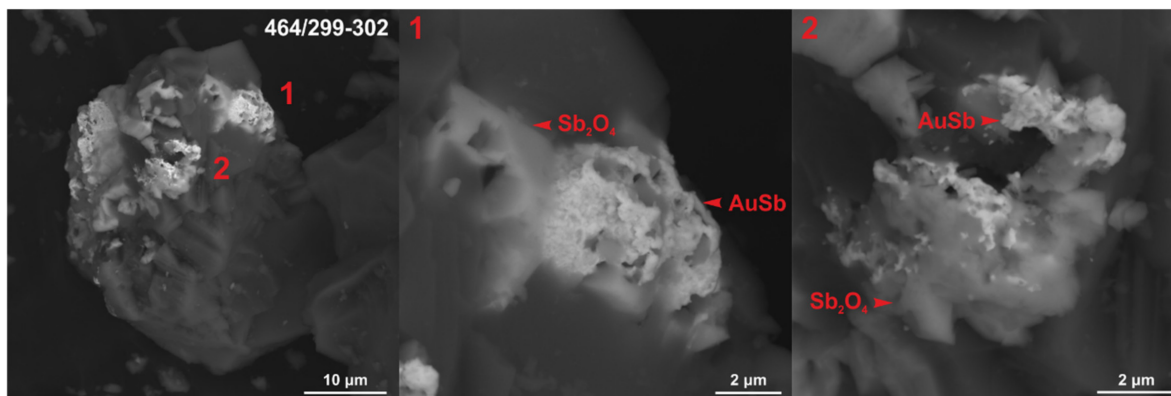
Figure 8. Products of aurostibite decomposition into spongiform gold and cervantite in the carbonate matrix of weathered bedrock of the deposit (the depth is 299–302 m—it is the deepest sample of the studied ones; see Figure 5).

Native gold from the oxidized ore samples is most often isolated in the form of independent particles, but its close aggregations with secondary iron minerals (especially in the upper part of the section) have been repeatedly observed. Figure 9 shows irregular shapes of a ferric (hydr)oxide grain (~10–100 μm) with numerous inclusions of native gold (up to 30 Au grains). The sizes of such inclusions vary widely from several hundreds of nanometers to 3–4 μm. As a rule, gold in such an association has rounded, smooth surfaces, and a single flattened crystal was found (Figure 9b). In addition, a mercurous gold inclusion was noted in tripuhyite.
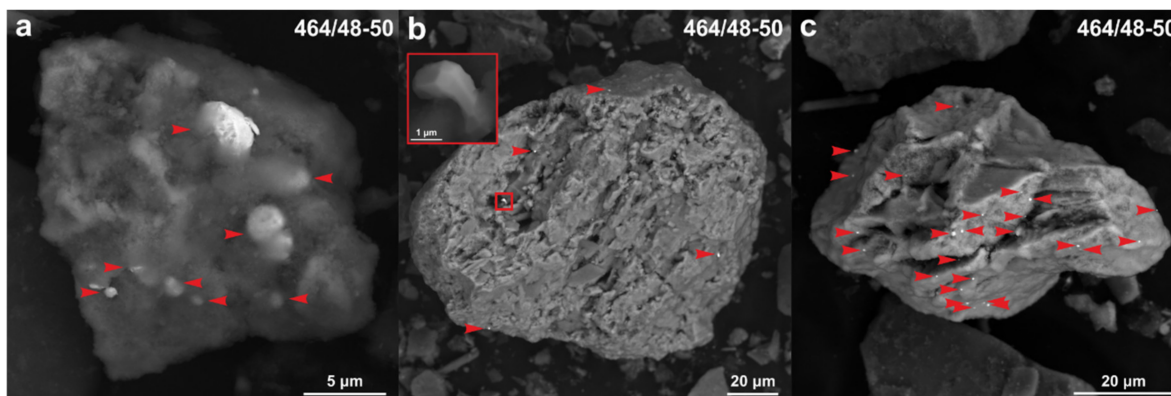
Figure 9. Inclusions of gold (red arrows) in ferric (hydr)oxides (**a**–**c**). The size of gold grains varies from 250 nm to 4 μm.

The SEM-EDS method was used for semi-quantitative (due to small size) determination of the chemical composition of the detected native gold. The overwhelming majority of chemical analyses of native gold in oxidized ores is characterized by the presence of O, Fe, Al, and Si (less often K, Ca, Mg, Mn, and Na). This is due to the presence of oxide and silicate films on gold particles, as well as the parasitic signal of the matrix on which the gold lies. Therefore, the impurities of these elements were not considered.

Among over 300 chemical composition determinations, sixteen analyses showed an impurity of Cu (0.8–10.7 wt.%), seventeen analyses showed Sb (0.5–35.2 wt.%), two showed Ag (3.1–4.2 wt.%) and five showed Hg (1.0–11.6 wt.%). At the same time, gold grains mainly contain only one impurity element. Reduced fineness is typical for spongiform gold and irregularly shaped gold of the lower part of the section. Gold with a mercury impurity has been noted here only. All studied crystals did not contain these impurities, except for one (2.9 wt.% Cu). Listed elements are typical impurities in native gold [51].

5. Discussion of the Oxidized Ores Formation Conditions

The specific geochemistry of the Olympiada oxidation zone is explained by the gold-antimony profile of primary ores (with W, Hg), which mainly served as the primary substrate (Figure 3a). Gold and associated metals were intensively redistributed, migrating from some horizons and accumulating in other horizons, which is controlled primarily by the sulfide content in the hypogene ores and pH and Eh of supergene solutions.

The main mineralogical and geochemical features of the selected horizons are as follows. The Lower Zone is distinguished by a significant accumulation of Au, usually in the form of spongiform gold, which appeared during the destruction of hypogene aurostibite, as well as wide development of supergene antimony and mercury minerals. The antimony concentrations here are maximum for the entire studied section. Oxidized ores of this zone inherit the geochemistry of parental gold-antimony ores to the maximum extent. The Middle Zone, on the contrary, is depleted with gold relative to the primary ores due to the intense removal of metal by oxidized fluids. The result of their activity is the dominance of kaoline and "hydromica" in the oxidized ores. Rare gold grains are represented here by globular shapes. Within the Middle Zone, there are local accumulations of alkali—lead (817 g/t) and copper (130 g/t)—generally not typical for the Olympiada oxidation zone. The Upper Zone has the most enriched ore level and differs in the maximum (up to 61 g/t) gold grade mainly present in the form of microcrystals. The highest concentrations of tungsten, silver and arsenic are also noted here. In the Upper Zone, we observe the maximum (up to several wt.%) sorption level of ore components (W, As, Sb) and metal gold nanoparticles on ferric (hydr)oxides. All of the above indicates a high mobility of supergene fluids in the formation of the oxidation zone, which led to its significant enrichment in the top part of the section [52].

As we have shown earlier [26], sulfide ores of the deposit contain mainly pyrite, pyrrhotite, arsenopyrite, stibnite and berthierite. Under exogenous conditions, these minerals are unstable and exposed to weathering. Oxidation of these sulfides led to the formation of sulfuric acid solutions and increased concentration of sulfate-ion and hydrogen-ion, which determined the reduction in pH and increase in the redox potential.

At the same time, the primary ores of the deposit contain a large amount of carbonates [26]. Dissociation of carbonate lead to neutralization of the acid on a large scale [53]. The combination of these factors led to fluctuations of redox conditions and acidity–alkalinity of the environment within the intensively oxidizing body of sulfide ores. Such a fluctuating area is most probable for the Middle and Upper Zones' boundary.

The existence of a geochemical barrier here is evidenced not only by the appearance of numerous newly formed crystals of native gold but also by the presence of supergene cerianite-(Ce) (Figure 6d). There is also an abrupt increase in Ce* values (up to ~1.1, Figure 5), which is probably caused by oxidation of the element to the low-soluble Ce^{4+} and its removal from aqueous solutions in the form of CeO_2 [54–60].

The kinetics of CeO_2 formation reactions strongly depends on pH and Eh, as well as on the participation of iron-oxidizing bacteria [61,62]. At the same time, it is reported that Ce, in contrast to most REE, has a greater affinity for Mn [63], and lower affinity for Fe [58], which is also noted in the samples studied (cerianite-(Ce) in association with manganese (hydr)oxides was detected). According to the data of the stability diagram of Ce-containing compounds in the Eh–pH coordinates [62], cerianite-(Ce) is stable in weakly reduced to strongly oxidized conditions with pH from 3 to 14. However, the negative Ce-anomaly in the solution (and, as a consequence, positive in the solid phase) is characteristic of the narrower CeO_2 stability field with Eh ~0.1–1.1 and pH ~3–7. On the other hand, there are data confirming that the negative anomaly of Ce occurs only in alkaline waters [64].

Oxidation of primary sulfides (arsenopyrite, pyrite, stibnite, aurostibite, etc., which are common in the primary ore paragenesis) leads to the formation of secondary minerals of Fe, Sb, As, Mn and Pb [5,11,13,65,66]. These minerals were detected in oxidized ore of deposit (see Table 1).

Thiosulphate-ion ($S_2O_3{}^{2-}$) is effective during dissolution and transportation of Au under near-neutral oxidizing conditions. It is assumed that the complex formation of Au with it is most likely during the oxidation of orogenic deposits [10,11]. The presence of thiosulfate radicals promotes the dissolution, mobilization and re-deposition of both gold, which is released from sulfides during their oxidation, and native Au^0 of bedrock ores. However, these complexes are metastable in the oxidizing environment, which leads to rapid deposition of Au^0 (together with ferric (hydr)oxides) and prevents the long-distance transfer of gold [5,67–70]. Chemical deposition of Au from thiosulfate complexes is possible either by their reduction during migration into not-yet-oxidized sulfide ores or during further oxidation with the formation of Fe hydroxides.

It is also believed that bacteria are capable of restoring the Au nanoparticles from thiosulfate complexes both inside and outside cells [17]. The interaction of $Au(S_2O_3)_2{}^{3-}$ with bacteria leads to the deposition of its nanoparticles, which are later able to aggregate into octahedral μ-crystals and/or spherical particles [16,71]. P.V. Bernatonis discovered bacteria of the *Thiobacillus ferrooxidans*, *Thiobacillus thiooxidans*, *Thiobacillus thiocyanooxidans*, *Thiobacillus thioparus* and *Thiobacillus denitrificans* species [43] in oxidized ores of the Olympiada deposit, which have contributed to gold redeposition.

Kashefi et al. also demonstrated that hyperthermophilic and mesophilic dissimilatory Fe(III)-reducing Bacteria and Archaea are capable of precipitating gold by reducing Au(III) to Au(0) with hydrogen as the electron donor in subsurface environments [72].

Trivalent complexes of gold Au(III)-OH-Cl-CN can exist in natural surface waters and may be important for the transport and biogeochemical cycling of gold in surface environments [11,73,74]. The possibility of the existence of Au(III)-Cl in the Upper Zone is consistent with the presence of Cl (up to 0.03 wt.%) here. Moreover, it was established earlier that 52% of mercury in the Olympiada oxidation zone exists in the chloride form [43].

In addition, a previous study showed that Au(III)-Cl complexes are adsorbed more readily onto iron oxides than are thio-Au(I) complexes [75]. This may indicate a lesser role of thiosulfate complexes in the deposition of Au in association with iron (hydr)oxides than is shown above. On the other hand, according to Gray and Pirlo, $AuCl_2{}^-$ is the dominant Au complex in Cl^- rich groundwaters [76]. In this case, the presence of dissolved Fe will reduce $AuCl_2{}^-$ [76].

Renders and Seward established the presence of $AuHS^0$, $Au(HS)_2{}^-$ and $Au_2S_2{}^{2-}$ in aqueous solutions (25 °C, pH 2–12, sulphur concentrations from 0.005 to 0.4 molal) [77]. We assumed that the presence of hydrosulfide gold complexes is most likely in the Lower Zone [5,11]. This complex was dominant form of the gold transport in aqueous-sulfide solutions during formation of primary ores [78].

The occurrence of spongiform gold in the Lower Zone is explained by the process of leaching of impurities (de-alloying), which is experimentally demonstrated in the work [79]. The formation of spongiform gold was also repeatedly observed in nature, as in the supergene zone during oxidation and decomposition of gold tellurides and antimonides,

as well as AuAg alloys [80–83] and under hypogene conditions under the influence of alkaline and neutral fluids with temperatures of 140–200 °C [84,85]. The liberation of gold from impurities in this process is accompanied by an increase in its free surface, which contributes to its further dissolution.

All this allows us to assert that the formation of oxidized ores of the Olympiada deposit took place under comprehensive geochemical conditions, in which Au behaved as a mobile element capable of redistribution and re-deposition on geochemical barriers (zone boundaries).

The formation of oxidized ores at the deposit is associated either with the development of a linear weathering crust or with late low-temperature hydrothermal-metasomatic activity. Apparently, both processes took place at the Olympiada deposit, and it is likely that hydrothermal and gas emanations were repeatedly superimposed on both primary ores and already existing weathering products. In contrast to the Cretaceous–Paleogene estimate of the age of linear weathering crusts at the Yenisei Ridge established in the literature, we tend to believe that the time interval of near-surface mineral formation at the Olympiada deposit may be hundreds of millions of years and primarily initiated by the activation of the Tatar Fault Zone when the Siberian craton collided with the Kazakhstan microcontinent on the border of the Devonian and Carboniferous ages. According to the data [86], the Paleogene-Quaternary spore and pollen spectra were found in the products of oxidized ores of the deposit from a depth of 5–28 m, gradually replaced at a depth of 30–60 m with the Mesozoic spectra and from a depth of 50–110 m with the Paleozoic (Permian, Carboniferous, Upper Devonian) spectra. The Upper Devonian age (368 ± 23 Ma Sm-Nd and 364 ± 7 Ma Rb-Sr based on fluorite) at the Yenisei Ridge has been established for the "telethermal" mineralization (calcite, barite, celestine, anhydrite, fluorite, realgar, smithsonite, cerussite, native silver) superimposed on the Neo-Proterozoic orogenic gold ores of the major Blagodatnoye deposit [87] and is assumed by us to be the beginning of the formation of the oxidation zone at the Olympiada deposit, unique in its composition.

The spatial combination of oxidized ores with the permeable zone of the Main Fault explains to a great extent a significant vertical span of oxidation products' development and does not exclude the influence of late low-temperature hydrotherms during their formation. Thus, methane and carbon dioxide emissions were recorded during drilling within the Eastern open pit in summer 2018, which lasted for two days. According to the geologists of JSC "Polyus Krasnoyarsk", thermal phenomena were repeatedly observed within the fault. This suggests that the Main Fault zone is still active and was able to supply portions of a low-temperature fluid to the near-surface zone of the deposit.

6. Conclusions

Supergene redistribution of gold and other components was detected in the section (to a depth of 300 m) of oxidized ores of the Olympiada deposit. The upper part of the section (Upper Zone) is the highest-grade (up to ~60 g/t of gold). In the Middle Zone, the noble metal content is minimal (~3 g/t). The lower part of the oxidized ores section (Lower Zone) is characterized by an average Au grade (~20 g/t). The boundaries of the identified zones are traced by a sudden change in the metal content.

Supergene and hypogene native gold have been identified. Crystalline individuals and their aggregates, as well as globules that predominate at the top of the section, are classified as supergene. The size of such crystals is quite uniform and averages 1 μm; the size of globular gold varies from several hundred nm to several μm. Flattened (fracture) gold particles of irregular morphology, occurring sporadically throughout the section, are relic hypogene. Spongiform gold is transitional from hypogene to supergene—it is a product of oxidation of aurostibite developed in the lower part of the section at the boundary with the bedrock, as well as in the bedrock, and formed in the process of leaching of impurities and further dissolution. Native gold of oxidized ores is commonly isolated, but close association with secondary iron minerals is typical for the newly formed globular and crystalline gold.

The obtained results suggest that the formation of oxidized ores was accompanied by the mobilization, redistribution and secondary enrichment of gold with the participation of both meteoric waters and low-temperature fluids.

Inflow of low-temperature (up to 200 °C) hydrothermal water, which leached the bedrock and sulfides (with the release of "invisible" gold) in the lower parts of the section, could occur along the permeable zone of the Main Fault upwards. The same fluids led to the removal of impurities from hypogene gold, as well as its partial dissolution and mobilization. It is assumed that stable $AuHS^0$ complex was present here, capable of migrating upwards at long distances together with the rising fluid. Partial destruction of these complexes was possible in the middle part of the section, which led to the formation of rare particles of newly formed globular and crystalline gold. Nanosize Au^0 extracted from sulfide minerals could also migrate upwards as colloids [88,89].

Meteoric waters coming from the day surface led to oxidation of sulfides and inversion of the redox potential in the Upper Zone. Leaching of sulfides was accompanied by local acidifying of the environment, which was neutralized in larger scales by the dissociation of carbonates and the arrival of new portions of meteoric water. The boundary of mixing of meteoric and low-temperature hydrothermal waters was the front of acid leaching and coincided with the boundary of the Middle and Upper Zones. Oxidation of sulfides in this part of the section was accompanied by the formation of thiosulphate complexes with released "invisible" as well as dissolving metal Au. Fluctuating changes in pH and Eh, as well as the influence of bacteria, led to the destruction of gold complexes and release of Au^0 in the form of micro- and nanoparticles, which were intensively sorbed on ferric (hydr)oxides appearing here, and agglomerated into larger crystalline and globular individuals. Ascending low-temperature fluids carrying $AuHS^0$ and probably gold colloids could facilitate secondary enrichment of the top of the section.

References

1. Smirnov, S.S. *Oxidation Zone of Sulfide Deposits*; Academy of Sciences USSR: Moscow, Russia, 1955; 232p. (In Russian)
2. Albov, M.N. *Secondary Zoning of the Gold Deposits of the Urals*; Gosgeoltekhizdat: Moscow, Russia, 1960; 215p. (In Russian)
3. Butt, C.R.M.; Smith, R.E. Conceptual models in exploration geochemistry: Australia. *J. Geochem. Explor.* **1980**, *12*, 89–365. [CrossRef]
4. González-Álvarez, I.; Anand, R.R.; Boni, M. Mineral exploration in regolith-dominated terrains. Global considerations and challenges. *Ore Geol. Rev.* **2016**, *73*, 375–379. [CrossRef]
5. Kalinin, Y.A.; Palyanova, G.A.; Naumov, E.A.; Kovalev, K.R.; Pirajnoe, F. Supergene remobilization of Au in Au-bearing regolith related to orogenic deposits: A case study from Kazakhstan. *Ore Geol. Rev.* **2019**, *109*, 358–369. [CrossRef]
6. Petrovskaya, N.V. *Native Gold*; Nauka: Moscow, Russia, 1973; 347p. (In Russian)
7. Greffie, C.; Benedetti, M.F.; Parron, C.; Amouric, M. Gold and iron oxide associations under supergene conditions: An experimental approach. *Geochim. Cosmochim. Acta.* **1996**, *60*, 1531–1542. [CrossRef]

8.　Kalinin, Y.A.; Kovalev, K.R.; Naumov, E.A.; Kirillov, M.V. Gold in the weathering crust at the Suzdal' deposit (Kazakhstan). *Russ. Geol. Geophys.* **2009**, *50*, 174–187. [CrossRef]

9.　Chapman, R.J.; Leake, R.C.; Bond, D.P.G.; Stedra, V.; Fairgrieve, B. Chemical and mineralogical signatures of gold formed in oxidizing chloride hydrothermal systems and their significance within populations of placer gold grains collected during reconnaissance. *Econ. Geol.* **2009**, *104*, 563–585. [CrossRef]

10.　Craw, D.; MacKenzie, D.; Grieve, P. Supergene gold mobility in orogenic gold deposits, Otago Schist, New Zealand. *N. Z. J. Geol. Geophys.* **2015**, *58*, 123–136. [CrossRef]

11.　Craw, D.; Kerr, G. Geochemistry and mineralogy of contrasting supergene gold alteration zones, southern New Zealand. *Appl. Geochem.* **2017**, *85*, 19–34. [CrossRef]

12.　Horbe, A.M.C.; Martins-Ferreira, M.A.C.; Lima, R.S. Supergene gold characterization by geochemistry, grain morphology and Au-Ag-Cu-Te classification. *J. South Am. Earth Sci.* **2019**, *95*, 102315. [CrossRef]

13.　Kalinin, Y.; Pal'yanova, G.; Bortnikov, N.; Naumov, E.; Kovalev, K. Aggregation and differentiation of gold and silver during the formation of the gold bearing regolith (on the example of Kazakhstan deposits). *Dokl. Earth Sci.* **2018**, *482*, 1193–1198. [CrossRef]

14.　Khusainova, A.S.; Gaskova, O.L.; Kalinin, Y.A.; Bortnikova, S.B. Physical-chemical model of gold conversion in products of ore processing of silver-polymetallic deposits (Salair Ridge, Russia). *Russ. Geol. Geophys.* **2020**, *61*(9), 964–975. [CrossRef]

15.　Amosov, R.A.; Vasin, S.L. Gold microfossils. *Ores Met.* **1993**, *3*, 101–107. (In Russian)

16.　Lengke, M.; Southam, G. Bioaccumulation of gold by sulfate-reducing bacteria cultured in the presence of gold(I)-thiosulfate complex. *Geochim. Cosmochim. Acta.* **2006**, *70*, 3646–3661. [CrossRef]

17.　Reith, F.; Etschmann, B.; Grosse, C.; Moors, H.; Benotmane, M.A.; Monsieurs, P.; Grass, G.; Doonan, C.; Vogt, S.; Lai, B.; et al. Mechanisms of gold biomineralization in the bacterium Cupriavidus metallidurans. *Proc. Natl. Acad. Sci. USA* **2009**, *106*, 17757–17762. [CrossRef]

18.　Zhmodik, S.M.; Kalinin, Y.A.; Roslyakov, N.A.; Belyanin, D.K.; Nemirovskaya, N.A.; Nesterenko, G.V.; Airiyants, E.V.; Moroz, T.N.; Bul'bak, T.A.; Mironov, A.G.; et al. Nanoparticles of noble metals in the supergene zone. *Geol. Ore Depos.* **2012**, *54*, 141–154. [CrossRef]

19.　Fairbrother, L.; Brugger, J.; Shapter, J.; Laird, J.S.; Southam, G.; Reith, F. Supergene gold transformation: Biogenic secondary and nano-particulate gold from arid Australia. *Chem. Geol.* **2012**, *320–321*, 17–31. [CrossRef]

20.　Reith, F.; Rea, M.A.D.; Sawley, P.; Zammit, C.M.; Nolze, G.; Reith, T.; Rantanen, K.; Bissett, A. Biogeochemical cycling of gold: Transforming gold particles from arctic Finland. *Chem. Geol.* **2018**, *483*, 511–529. [CrossRef]

21.　Sanyal, S.K.; Shuster, J.; Reith, F. Cycling of biogenic elements drives biogeochemical gold cycling. *Earth Sci. Rev.* **2019**, *190*, 131–147. [CrossRef]

22.　Rea, M.A.; Shuster, J.; Hoffmann, V.E.; Schade, M.; Bissett, A.; Reith, F. Does the primary deposit affect the biogeochemical transformation of placer gold and associated biofilms? *Gondwana Res.* **2019**, *73*, 77–95. [CrossRef]

23.　Boyle, R.W. An occurrence of native gold in an ice lens; giant-Yellowknife gold mines, Yellowknife, Northwest Territories. *Econ. Geol.* **1951**, *46*, 223–227. [CrossRef]

24.　Shvartsev, S.L. A possible mechanism for the formation of native gold in ice lenses. *Bull. Tomsk Polytech. Inst.* **1976**, *289*, 107–109. (In Russian)

25.　Reith, F.; Brugger, J.; Zammit, C.M.; Nies, D.H.; Southam, G. Geobiological cycling of gold: From fundamental process understanding to exploration solutions. *Minerals* **2013**, *3*, 367–394. [CrossRef]

26.　Sazonov, A.M.; Lobanov, K.V.; Zvyagina, E.A.; Leontiev, S.I.; Silyanov, S.A.; Nekrasova, N.A.; Nekrasov, A.Y.; Borodushkin, A.B.; Poperekov, V.A.; Zhuravlev, V.V.; et al. Olympiada gold deposit, Yenisei Ridge, Russia. *Econ. Geol.* **2020**. In press.

27.　Kuzmichev, A.B.; Sklyarov, E.V. The precambrian of transangaria, Yenisei Ridge (Siberia): Neoproterozoic microcontinent, Grenville-age orogen, or reworked margin of the Siberian craton? *J. Asian Earth Sci.* **2016**, *115*, 419–441. [CrossRef]

28.　Nozhkin, A.D.; Borisenko, A.S.; Nevol'ko, P.A. Stages of Late Proterozoic magmatism and periods of Au mineralization in the Yenisei Ridge. *Russ. Geol. Geophys.* **2011**, *52*, 124–143. [CrossRef]

29.　Novozhilov, Y.I.; Gavrilov, A.M. *Gold-Sulfide Deposits in Carbon-Terrigenous Strata*; TsNIGRI: Moscow, Russia, 1999; 175p. (In Russian)

30.　Lee, L.V. *Olimpiadinskoe Deposit of Disseminated Gold-Sulfide Ores*; KNIIGiMS: Krasnoyarsk, Russia, 2003; 120p. (In Russian)

31.　Savichev, A.A.; Shevchenko, S.S.; Rozinov, M.I.; Lokhov, K.I.; Prasolov, E.M.; Prilepskiy, E.B.; Kapitonov, I.N.; Matukov, D.I.; Berezhnaya, N.G.; Sergeev, S.A. Isotope-geochemical characteristics of the gold-sulfide deposits of the Olympics and its satellites (Yenisei Ridge). *Reg. Geol. Metallog.* **2006**, *26*, 122–143. (In Russian)

32.　Gibsher, N.A.; Sazonov, A.M.; Travin, A.V.; Tomilenko, A.A.; Ponomarchuk, A.V.; Sil'yanov, S.A.; Nekrasova, N.A.; Shaparenko, E.O.; Ryabukha, M.A.; Khomenko, M.O. Age and duration of the formation of the Olimpiadinski gold deposit (Yenisei ridge, Russia). *Geochem. Int.* **2019**, *57*, 593–599. [CrossRef]

33.　Gibsher, N.A.; Tomilenko, A.A.; Sazonov, A.V.; Bul'bak, T.A.; Ryabukha, M.A.; Sil'yanov, S.A.; Nekrasova, N.A.; Khomenko, M.O.; Shaparenko, E.O. The Olimpiada gold deposit (Yenisei ridge): Temperature, pressure, composition of ore-forming fluids, $\delta^{34}S$ in sulfides, $^3He/^4He$ of fluids, Ar-Ar age and duration of deposit formation. *Russ. Geol. Geophys.* **2019**, *9*, 1310–1330. [CrossRef]

34.　Sazonov, A.M.; Zvyagina Ye, A.; Silyanov, S.A.; Lobanov, K.V.; Leontyev, S.I.; Kalinin Yu, A.; Savichev, A.A.; Tishin, P.A. Ore genesis of the Olimpiada gold deposit (Yenisei Ridge, Russia). *Geosph. Res.* **2019**, 17–43. [CrossRef]

35. Savichev, A.A.; Gavrilenko, V.V. Gold-sulfide mineralization of the North Yenisei region (Siberia) and the conditions for its formation. *Notes All-Russ. Mineral. Soc.* **2003**, *2*, 15–32. (In Russian)

36. Belyi, A.V.; Chernov, D.V.; Solopova, N.V. Development of BIONORD®technology on Olimpiada deposit refractory arsenic-gold ores treatment in conditions of Extreme North. *Hydrometallurgy* **2018**, *179*, 188–191. [CrossRef]

37. Genkin, A.D.; Bortnikov, N.S.; Cabri, L.J.; Wagner, F.E.; Stanley, C.J.; Safonov, Y.G.; McMahon, G.; Friedl, J.; Kerzin, A.L.; Gamyanin, G.N. A multidisciplinary study of invisible gold in arsenopyrite from four mesothermal gold deposits in Siberia, Russian Federation. *Econ. Geol.* **1998**, *93*, 463–487. [CrossRef]

38. Sazonov, A.M.; Silyanov, S.A.; Bayukov, O.A.; Knyazev, Y.V.; Zvyagina, Y.A.; Tishin, P.A. Composition and ligand microstructure of arsenopyrite from gold ore deposits of the Yenisei Ridge (Eastern Siberia, Russia). *Minerals* **2019**, *9*, 737. [CrossRef]

39. Trigub, A.L.; Tagirov, B.R.; Kvashnina, K.O.; Chareev, A.; Nickolsky, M.S.; Shiryaev, A.A.; Baranova, N.N.; Kovalchuk, E.V.; Mokhov, A.V. X-ray spectroscopy study of the chemical state of "invisible" Au in synthetic minerals in the Fe-As-S system. *Am. Miner.* **2017**, *102*, 1057–1065. [CrossRef]

40. Merkulova, M.; Mathon, O.; Glatzel, P.; Rovezzi, M.; Batanova, V.; Marion, P.; Boiron, M.-C.; Manceau, A. Revealing the chemical form of "invisible" gold in natural arsenian pyrite and arsenopyrite with high energy-resolution X-ray absorption spectroscopy. *ACS Earth Space Chem.* **2019**, *3*, 1905–1914. [CrossRef]

41. Peskov, E.G. *Geological Manifestations of Cold Degassing of the Earth*; SVKNII FEB RAS: Magadan, Russia, 2000; 279p. (In Russian)

42. Yablokova, S.V.; Konovalova, M.S.; Sandomirskaya, S.M. Mineralogy of the gold-bearing weathering crust in the deposits of vein-disseminated sulfide ores in terrigenous-carbonate strata of the Precambrian. *Tr. TSNIGRI* **1986**, *208*, 10–19. (In Russian)

43. Bernatonis, P.V. Oxidation Zone of the Olympiadinsky Vein-Disseminated Gold-Sulfide Deposit. Ph.D. Thesis, Tomsk Polytechnic University, Tomsk, Russia, 1999. (In Russian).

44. Sergeev, N.B. Features of the structure and material composition of the gold-bearing weathering crust (Yenisei ridge). *Weather. Crust* **1991**, *20*, 77–90. (In Russian)

45. Genkin, A.D.; Lopatin, V.A.; Saveliev, R.A.; Safonov, Y.G.; Sergeev, N.B.; Kerzin, A.L.; Tsepin, A.I.; Amshutts, H.; Afanasyeva, Z.B.; Wagner, F.; et al. Gold ores of the Olympiada deposit (Yenisei Ridge. Siberia). *Geol. Ore Depos.* **1994**, *3*, 111–136. (In Russian)

46. Sergeev, N.B.; Zvezdinskaya, L.V.; Sergeeva, V.V. Tungsten containing hydroromeit—A new mineral variety from Eastern Siberia. *Rep. RAS.* **1993**, *332*, 99–101. (In Russian)

47. Afanas'eva, Z.B.; Ivanova, G.F.; Raimbault, L.; Miklishanskii, A.Z. Rare-earth geochemistry of rocks and minerals from the olimpiada scheelite-bearing Gold Sulfide Deposit, Yenisei Ridge, Russia. *Geochem. Int.* **1997**, *35*, 155–166.

48. Zvyagina, E.A. Metamorphism and Gold Metallogeny of the Upper Enashimo ore Cluster. Ph.D. Thesis, Siberian Federal University, Krasnoyarsk, Russia, 1989. (In Russian).

49. Sazonov, A.M.; Zvyagina, E.A.; Silyanov, S.A.; Babenkov, D.E. Gold in the Olimpiada mine ore and tailings. *Gorn. Zhurnal.* **2019**, *4*, 54–59. [CrossRef]

50. Roslyakov, N.A. *Geochemistry of Gold in Supergene Zone*; Nauka: Novosibirsk, Russia, 1981; 240p. (In Russian)

51. Palyanova, G.A. Gold and silver minerals in sulfide Ore. *Geol. Ore Depos.* **2020**, *62*, 426–449. [CrossRef]

52. Kalinin, Y.A.; Roslyakov, N.A. Geochemistry of noble, rare and radioactive elements in exogenous ore-forming systems. In *The History of the Development of the Institute of Geology and Geophysics SB (USSR Academy of Sciences and RAS) and Its Scientific Directions*; SS RAS: Novosibirsk, Russia, 2010; pp. 503–511.

53. Craw, D. Water–rock interaction and acid neutralization in a large schist debris dam, Otago, New Zealand. *Chem. Geol.* **2000**, *171*, 17–32. [CrossRef]

54. Chudaeva, V.A.; Chudaev, O.V. Accumulation and fractionation of rare earth elements in surface waters of the Russian Far East under the conditions of natural and anthropogenic anomalies. *Geochem. Int.* **2011**, *49*, 498–524. [CrossRef]

55. Radomskaya, V.I.; Radomskii, S.M.; Kulik, E.N.; Rogulina, L.I.; Shumilova, L.P.; Pavlova, L.M. Geochemical features of rare-earth elements in surface and subsurface waters in the field of the Albynskoe Gold-Bearing Placer, Amur oblast. *Water Resour.* **2017**, *44*, 284–296. [CrossRef]

56. Braun, J.J.; Pagel, M.; Muller, J.P.; Bilong, P.; Michaud, A.; Guillet, B. Cerium anomalies in lateritic profiles. *Geochim. Cosmochim. Acta* **1990**, *51*, 597–605. [CrossRef]

57. Koppi, A.J.; Edis, R.; Field, D.J.; Geering, H.R.; Klessa, D.A.; Cockayne, D.J.H. Rare earth trends and cerium-uranium-manganese association in weathered\rock from Koongarra, Northern Territory, Australia. *Geochim. Cosmochim. Acta.* **1996**, *60*, 1695–1707. [CrossRef]

58. Bau, M. Scavenging of dissolved yttrium and rare earths by precipitating iron oxyhydroxide: Experimental evidence for Ce oxidation, Y-Ho fractionation and lanthanide tetrad effect. *Geochim. Cosmochim. Acta.* **1999**, *63*, 67–77. [CrossRef]

59. Ohta, A.; Kawabe, I. REE(III) adsorption onto Mn dioxide (-MnO_2) and Fe oxyhydroxide: Ce(III) oxidation by δ-MnO_2. *Geochim. Cosmochim. Acta* **2001**, *65*, 695–703. [CrossRef]

60. Seto, M.; Akagi, A. Chemical condition for the appearance of a negative Ce anomaly in stream waters and groundwaters. *Geochem. J.* **2008**, *42*, 371–380. [CrossRef]

61. Moffett, J.W. Microbially mediated cerium oxidation in sea water. *Nature* **1990**, *345*, 421–423. [CrossRef]

62. Akagi, T.; Masuda, A. A simple thermodynamic interpretation of Ce anomaly. *Geochem. J.* **1998**, *32*, 301–314. [CrossRef]

63. Kawabe, I.; Ohta, A.; Ishu, S.; Tokumura, M.; Miyauchi, K. REE portioning between precipitates and weakly acid NaCl solutions: Convex tetrad effect and fractionation of Y and Sc from heavy lanthanides. *Geochem. J.* **1999**, *33*, 167–179. [CrossRef]

64. Elderfield, H.; Upstill-Goddard, R.; Sholkovitz, E.R. The rare earth elements in rivers, estuaries, and coastal seas and their significance to the composition of the ocean waters. *Geochim. Cosmchim. Acta* **1990**, *54*, 971–991. [CrossRef]

65. Reith, F.; Lengke, M.F.; Falconer, D.; Craw, D.; Southam, G. The geomicrobiology of gold. *ISME J.* **2007**, *1*, 567–584. [CrossRef] [PubMed]

66. Radkova, A.B.; Jamieson, H.E.; Campbell, K.M. Antimony mobility during the early stages of stibnite weathering in tailings at the Beaver Brook Sb deposit, Newfoundlend. *J. Appl. Geochem.* **2020**, *115*, 104528. [CrossRef]

67. Shabynin, L.L. On the issue of migration of gold in an aqueous medium in thiosulfate form. *Izv. Tomsk Polytech. Inst.* **1967**, *67*, 67–72. (In Russian)

68. Webster, J.G. The solubility of gold and silver in the system Au–Ag–S–O_2–H_2O at 25 °C and 1 atm. *Geochim. Cosmochim. Acta* **1986**, *50*, 1837–1845. [CrossRef]

69. Stezeryanskii, E.; V'yunov, O.; Omelchuk, A. Determination of the stability constants of gold(I) thiosulfate complexes by differential UV spectroscopy. *J. Solut. Chem.* **2015**, *44*, 1749–1755. [CrossRef]

70. Kerr, G.; Craw, D. Mineralogy and geochemistry of biologically-mediated gold mobilisation and redeposition in a semiarid climate, Southern New Zealand. *Minerals* **2017**, *7*, 147. [CrossRef]

71. Reith, F.; Stewart, L.; Wakelin, S.A. Supergene gold transformation: Secondary and nano-particulate gold from southern New Zealand. *Chem. Geol.* **2012**, *320–321*, 32–45. [CrossRef]

72. Kashefi, K.; Tor, J.M.; Nevin, K.P.; Lovley, D.R. Reductive precipitation of gold by dissimilatory Fe(III)-reducing Bacteria and Archaea. *Appl. Environ. Microbiol.* **2001**, *67*, 3275–3279. [CrossRef] [PubMed]

73. Cohen, D.R.; Waite, T.D. Interaction of aqueous Au species with goethite, smectite and kaolinite. *Geochem.-Explor. Env. A* **2004**, *4*, 279–287. [CrossRef]

74. Ta, C.; Reith, F.; Brugger, J.; Pring, A.; Lenehan, C. Analysis of gold(I/III)-complexes by HPLC-ICP-MS demonstrates gold(III) stability in surface waters. *Environ. SciTech.* **2014**, *48*, 5737–5744. [CrossRef]

75. Ran, Y.; Fu, J.; Rate, A.W.; Gilkes, R.J. Adsorption of Au(I, III) complexes on Fe, Mn oxides and humic acid. *Chem. Geol.* **2002**, *1–2*, 33–49. [CrossRef]

76. Gray, D.J.; Pirlo, M.C. *Hydrogeochemistry of the Tunkillia Gold Prospect, South Australia*; CRC LEME Open File Report 194; CRC LEME: Wembley, Australia, 2005; 109p.

77. Renders, P.; Seward, T. The stability of hydrosulphido- and sulphido-complexes of Au(I) and Ag(I) at 25 °C. *Geochim. Cosmochim. Acta* **1989**, *53*, 245–253. [CrossRef]

78. Pal'yanova, G. Physicochemical modeling of the coupled behavior of gold and silver in hydrothermal processes: Gold fineness, Au/Ag ratios and their possible implications. *Chem. Geol.* **2008**, *255*, 399–413. [CrossRef]

79. Schofield, E.J.; Ingham, B.; Turnbull, A.; Toney, M.F.; Ryan, M.P. Strain development in nanoporous metallic foils formed by dealloying. *Appl. Phys. Lett.* **2008**, *92*, 043118. [CrossRef]

80. Makovicky, E.; Chovan, M.; Bakos, F. The stibian mustard gold from the Kriván Au deposit, Tatry Mts., Slovak Republic. *N. Jb. Miner. Abh.* **2007**, *184*, 207–215. [CrossRef]

81. Tolstykh, N.D.; Palyanova, G.A.; Bobrova, O.V.; Sidorov, E.G. Mustard gold of the gaching Ore deposit (Maletoyvayam Ore Field, Kamchatka, Russia). *Minerals* **2019**, *9*, 489. [CrossRef]

82. Kalinin, A.A.; Savchenko, Y.E.; Selivanova, E.A. Mustard gold in the oleninskoe gold deposit, Kolmozero–Voronya Greenstone Belt, Kola Peninsula, Russia. *Minerals* **2019**, *9*, 786. [CrossRef]

83. Anisimova, G.S.; Kondratieva, L.A.; Kardashevskaia, V.N. Characteristics of supergene gold of Karst Cavities of the Khokhoy Gold Ore Field (Aldan Shield, East Russia). *Minerals* **2020**, *10*, 139. [CrossRef]

84. Zhao, J.; Bruger, J.; Gundler, P.V.; Xia, F.; Chen, G.; Pring, A. Mechanism and kinetics of a mineral transformation under hydrothermal conditions: Calaverite to metallic gold. *Am. Miner.* **2009**, *94*, 1541–1555. [CrossRef]

85. Okrugin, V.M.; Andreeva, E.; Etschmann, B.; Pring, A.; Li, K.; Zhao, J.; Gri_ths, G.; Lumpkin, G.R.; Triani, G.; Brugger, J. Microporous gold: Comparison of textures from nature and experiments. *Am. Mineral.* **2014**, *99*, 1171–1174. [CrossRef]

86. Storozhenko, A.A.; Vasiliev, N.F.; Diner, A.E.; Pimanov, A.V.; Trofimov, Y.P.; Gursky, Y.I.; Pimanova, G.P.; Kiseleva, E.A.; Borodushkin, A.B. *State Geological Map of the Russian Federation on a Scale of 1: 200 000*, 2nd ed.; Series Yenisei. Sheet O-46-III. Explanatory Letter; Cartographic Factory VSEGEI: St. Petersburg, Russia, 2002; 125p. (In Russian)

87. Sazonov, A.M.; Gertner, I.F.; Zvyagina, E.A.; Tishin, P.A.; Poleva, T.V.; Leontyev, S.I.; Kolmakov, Y.V.; Krasnova, T.S. Ore-forming conditions of the Blagodat Gold Deposit in the Riphean Metamorphic Rocks of the Yenisey Ridge according to geochemical and isotopic data. *J. Sib. Fed. Univ. Eng. Technol.* **2009**, *2*, 203–220. (In Russian)

88. Goleva, G.A.; Krivenkov, V.A.; Gudz, Z.G. Geochemical regularities of the distribution and forms of migration of gold in natural waters. *Geokhimiya* **1970**, *6*, 744–757. (In Russian)

89. Ong, H.L.; Swanson, V.E. Natural organic acids in the transportation, deposition, and concentration of gold. *Q. Colo. Sch. Mines.* **1969**, *64*, 395–425.